MULTI-COMPONENT SIMULATION AND KINETICS MODEL FOR CO-COMBUSTION OF HUADIAN OIL SHALE RETORTING RESIDUE AND CORNSTALKS

LIU HONGPENG[a], SUN XIAOJIAN[a], WANG XUDONG[b], WANG QING[a]*

[a] Engineering Research Centre of Oil Shale Comprehensive Utilization, Ministry of Education, School of Energy and Power Engineering, Northeast Dianli University, Jilin, 132012, Jilin Province, China
[b] Shenhua Guohua (Zhoushan) Power Generation Co., Ltd, Zhoushan 316012, Zhejiang Province, China

Abstract: *A series of experiments on co-combustion of the retorting residue of Huadian oil shale and cornstalks at different blending proportions were performed on a Pyris-1 thermogravimetric analyzer (TGA) to investigate the mechanism of the reactions involved. Moreover, the abrupt curvature changes of thermogravimetric (TG) curves and the multi-peaks and -shoulders of differential thermal gravity (DTG) curves for the blends were analyzed based on a simulation model of multi-component combustion. Results showed that the processes of combustion represented a multistage procedure of a clearly segmented nature. The processes can be divided into three stages of different temperature ranges: the first stage (135–380 °C), the second stage (380–560 °C) and the third stage (560–700 °C). With increasing blending ratio of cornstalks, the free energy of activation of combustion in the first and second stages is much lower than that in the third stage. Meanwhile, the continuous reaction processes of the samples combustion were analyzed by the Kissinger-Akahira-Sunose (KAS) kinetics model. Results showed that the activation enthalpy, activation entropy and free energy of activation of the samples combustion in its different stages varied. Moreover, with the addition of cornstalks, the portion of the ordered structure of activated molecules increased and the combustion characteristics of the retorting residue improved.*

Keywords: *multi-component combustion, KAS kinetics model, activation enthalpy, activation entropy, free energy of activation.*

---

* Corresponding author: e-mail *rlx888@126.com*

1. Introduction

With abundant reserves, oil shale is an important alternative or supplement resource to the conventional oil and gas resource [1]. However, the retorting residue, generated in the oil refining process at oil shale retorting, is huge in quantities, possessing at the same time a certain calorific value [2]. Its leachates contain some phenolic compounds, sulfides, polycyclic aromatics, etc., as well as certain toxic trace elements like P_b and C_d, which can cause severe damage to the environment [3]. So, these drawbacks have been a bottleneck in the further development and utilization of oil shale.

Therefore, in recent years a great deal of research has been conducted by scientists worldwide on how to effectively dispose of the oil shale retorting residue (or semi-coke). Kuusik et al. studied the fluidized-bed combustion of oil shale retorting residue and found that for semi-coke with a moisture content more than 10%, about 10% of oil shale must be involved to make it burn [4]. Gil et al. investigated the thermal characteristics and kinetics of coal and biomass and their blends by using TGA, and found that the blends underwent three combustion stages [5]. Zanoni et al. formulated and optimized the chemical combustion mechanism of oil shale and its semi-coke and successfully estimated the kinetic parameters which affect drying, pyrolysis, oxidation and decarbonation reactions [6]. Wang et al. analyzed the kinetics of Huadian oil shale and the co-combustion performance of its semi-coke and cornstalks by the Distributed Activation Energy Model (DAEM) [7, 8]. Sun et al. investigated the kinetics of co-combustion of oil shale semi-coke and bituminous coal by the Flynn-Wall-Ozawa (FWO) method and the inference method of Popescu mechanism function and established the most optimum mechanism for this function model [9].

Now, researches on co-combustion of oil shale retorting residue and bio-mass are relatively few. Biomass energy resource is abundant; in addition, biomass burning generates lower amounts of ash, pollutants and net CO_2 emissions. However, due to that biomass is mostly abandoned or burnt directly, the environmental pollution may also be quite serious. Therefore, not only can the co-combustion of oil shale retorting residue and biomass fully utilize the resource, environmental hazards can also be diminished [10, 11]. Meanwhile, the popularity of low-carbon policies makes fuels co-combustion techniques more attractive, hence the co-combustion of oil shale retorting residue and biomass is a promising trend, especially in China [5, 12].

This paper proposes a project for combustion of oil shale retorting residue (SC) and cornstalks (CS) blends. The combustion processes of the blends were investigated by TGA, and the mechanisms of the reactions of the blends at different blending ratios were studied. On the basis of the curvature changes of TG curves and the multi-peaks and -shoulders of DTG curves for the combustion, the study employed the transformation dynamics theory to describe the sample components conversion in different temperature ranges.

Moreover, the transition state theory and KAS dynamics model were also used to investigate the energy triplet of the activated complex in the combustion processes. Applying the above two theories and KAS dynamics model, the study analyzed the mechanisms of co-combustion reactions of sample components in more detail.

2. Experimental section

2.1. Materials and sample preparation

The samples used in this work were Huadian oil shale retorting residue and cornstalks, obtained from Huadian in Jilin Province, China. The samples were milled and sieved to obtain particles with a size less than 0.2 mm according to ASTM standards. The labels and component proportions of blending samples are given in Table 1. The results of proximate and ultimate analyses of the samples on air dried basis are presented in Table 2. The proximate analysis was performed using an SDLA718 Industrial Analyzer (Sundy, China), the ultimate analysis was performed using a EURO EA3000 Elemental Analyzer.

Table 1. Labels and component proportions of blending samples

Sample label	M_1	M_2	M_3	M_4	M_5	M_6	M_7
SC : CS	10:0	9:1	8:2	7:3	6:4	5:5	0:10

Table 2. Proximate and ultimate analyses of oil shale semi-coke and cornstalk samples

Sample	Proximate analysis, %				$Q_{net,ar}$, kJ/kg	Ultimate analysis, %				
	M_{ad}	V_{ad}	A_{ad}	FC_{ad}		C_{ad}	H_{ad}	O_{ad}	N_{ad}	S_{ad}
SC	0.89	10.44	82.62	6.09	3 868.29	11.29	0.35	4.21	0.11	0.53
CS	7.39	69.86	6.06	16.68	17 097.38	37.95	6.47	40.76	0.77	0.59

2.2. Experimental setup

The experiments were performed on the Pyris1-1 TGA (Perkin Elmer, USA). In order to diminish the effect of temperature and concentration gradients, 6 mg of sample was placed evenly at the bottom of an Al_2O_3 ceramic crucible. In a simulated air state (80 mL/min), the samples were heated from 40 °C up to 850 °C at different blending ratios and certain heating rates (10, 20, 50, 80 °C/min). A thermobalance automatically heated at a set heating rate and recorded the signals of change of combustion curves.

3. TG curves of SC/CS combustion

The combustion characteristics of SC and CS were investigated at different blending ratios. The TG and DTG curves for the blending samples M_1 to M_7 are shown in Figures 1a and 1b at a heating rate of 20 °C/min. Figure 2 shows the DTG curves of sample M_4 at different heating rates (10, 20, 50, 80 °C/min).

As seen from Figures 1 and 2, the combustion of blending samples involved three major processes: moisture release, light hydrocarbon combustion, and combustion of difficult-to-decompose organic matter and coke [13, 14]. As shown in Figure 1, with increasing blending ratio of CS, the characteristic curves of combustion moved toward low temperature areas, and the burnout temperature of samples decreased. This could be attributed to the increase of light hydrocarbon contributing to the burnout of samples
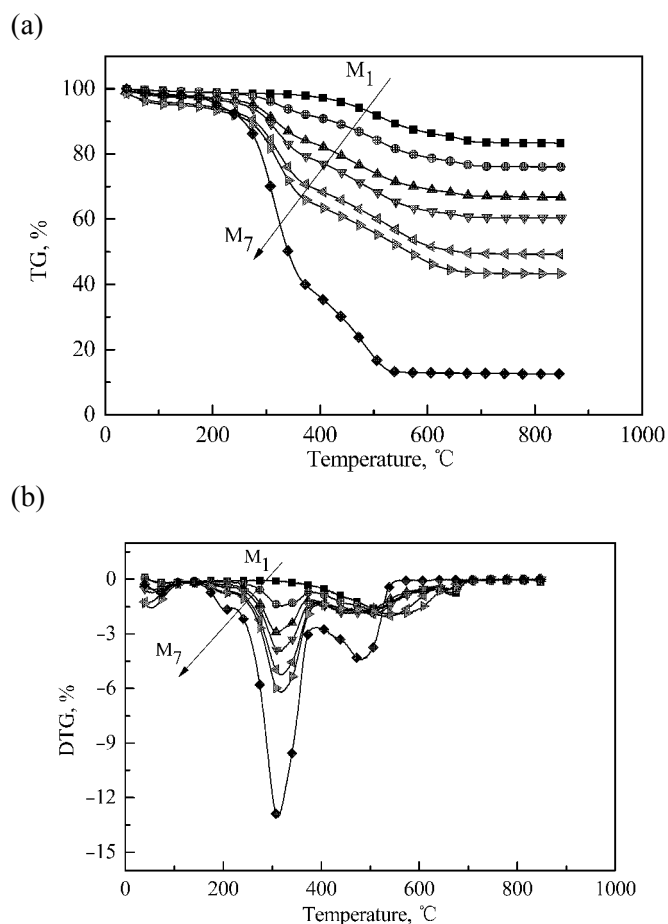
(a)

(b)

Fig. 1. (a) TG curves and (b) DTG curves of blending samples M_1 to M_7.
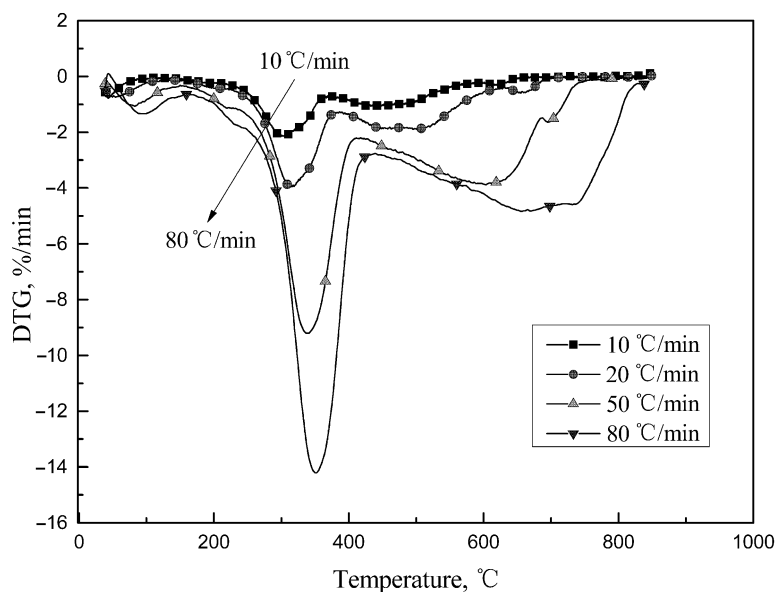
Fig. 2. DTG curves of the blending sample M_4.

particles. As demonstrated in Figure 2, with the increase of heating rate, the curves of combustion moved toward high temperature areas, and the burnout temperature of samples increased, while their burnout degree decreased. This was due to the increase of difference between the interior and exterior temperatures of samples particles which blocked the release and burning of the light hydrocarbon. As a result, oxygen gas could not fully diffuse into the inside of samples particles and therefore their combustion performance worsened.

4. Combustion kinetics of SC/CS blends

4.1. Combustion kinetics of blend components

García and Font, and Várhegyi et al. investigated the mechanism of fuels combustion and found that when fuel samples were burning, their weight loss of varying degrees occurred in every temperature range. The weight loss was reflected on TG curves as curvature variations, while on DTG curves it was expressed as "shoulders" or "peaks". This occurred due to the fuel samples containing components of different structure [15, 16].

From the curvature changes of TG curves and the multi-peaks and -shoulders on DTG curves it can be concluded that the combustion processes of blending samples represented a multi-stage burning with the complex of components involved, and consisted of moisture release, light hydrocarbon combustion and combustion of difficult-to-decompose organic matter and coke. To describe in more detail the mechanism of combustion of samples

components in a continuous reaction process, the TG curves simulation, based on the kinetics of solid particles decomposition, was used in this research.

A kinetic theory devised by Johnson and Avrami has been applied to analyze solid particles combustion [17–19], and can be expressed as follows:

$$\alpha = 1 - \exp\left[-g\int_0^t I_v \left(\int_{t'}^t u \, d\tau \right)^m dt' \right], \tag{1}$$

where α is the conversion ratio, t is the time, g is the shape factor, I_v is the nucleation frequency per unit of volume of substance, u is the growth rate, m is an integer which depends on the mechanism of a reaction.

Integrated by Johnson and Avrami, the above equation leads to Equation (2):

$$\begin{aligned} \alpha &= 1 - \exp[-(kt)^n] \\ T &= T_0 + \beta t \end{aligned} \tag{2}$$

Introducing the transition state theory [20, 21] we can get Equation (3):

$$\begin{aligned} k &= \frac{Rt}{hN_A} K^{\neq} \\ \Delta G_{\neq}^{\Theta} &= \Delta H_{\neq}^{\Theta} - T\Delta S_{\neq}^{\Theta} = -RT \ln K^{\neq} \end{aligned} \tag{3}$$

Combining Equation (2) with Equation (3) gives Equation (4):

$$\alpha = 1 - \exp\left[-\left(\frac{RT}{N_A h} \exp(-\Delta G_{\neq}^{\Theta}/RT)(T-T_0)/\beta \right)^n \right], \tag{4}$$

where N_A is Avogadro's constant, h is Planck's constant, T_0 is the initial temperature of the reaction, β is heating rate. From Equations (3) and (4) we can get Equation (5) used in the simulation of TG curves:

$$w(T) = 1 - \alpha = \sum_{i=1}^m w_i \exp\left[-\left(\frac{RT}{N_A h} \exp(-\Delta G_{\neq}^{\Theta}/RT)(T-T_0)/\beta \right)^{n_i} \right], \tag{5}$$

where $w(T)$ is the percentage of residual mass, w_i is the initial mass fraction on stage i, $(\Delta G_{\neq}^{\Theta})_i$ is the free energy of activation of a reaction, n_i is the order of a reaction, m is the stage number of a reaction, and w_i satisfies Equation (6):

$$\sum_{i=1}^m w_i = 1. \tag{6}$$

Equation (5) is used in this research to simulate the TG curves of samples combustion.

4.2. Simulation of TG curves of SC/CS

According to the peaks and shoulders of DTG curves, the combustion of every blending sample represents a multicomponent process. It could be approximately subdivided into three stages: the first stage (135–380 °C) is the release and combustion of volatile substances of CS, the second stage (380–560 °C) is the co-combustion of fixed carbon of CS and volatiles of SC, and the third stage (560–700 °C) is the combustion of fixed carbon of SC.

Figure 3 shows the results of the simulation of TG curves for blending samples M_2–M_6 at a heating rate of 20 °C/min. The specific simulation parameters are presented in Table 3.

From Figure 3 it is seen that with the increase of the blending ratio of CS, the sample components interaction effects in the first and second stages of combustion became more pronounced. This could be attributed to the fixed
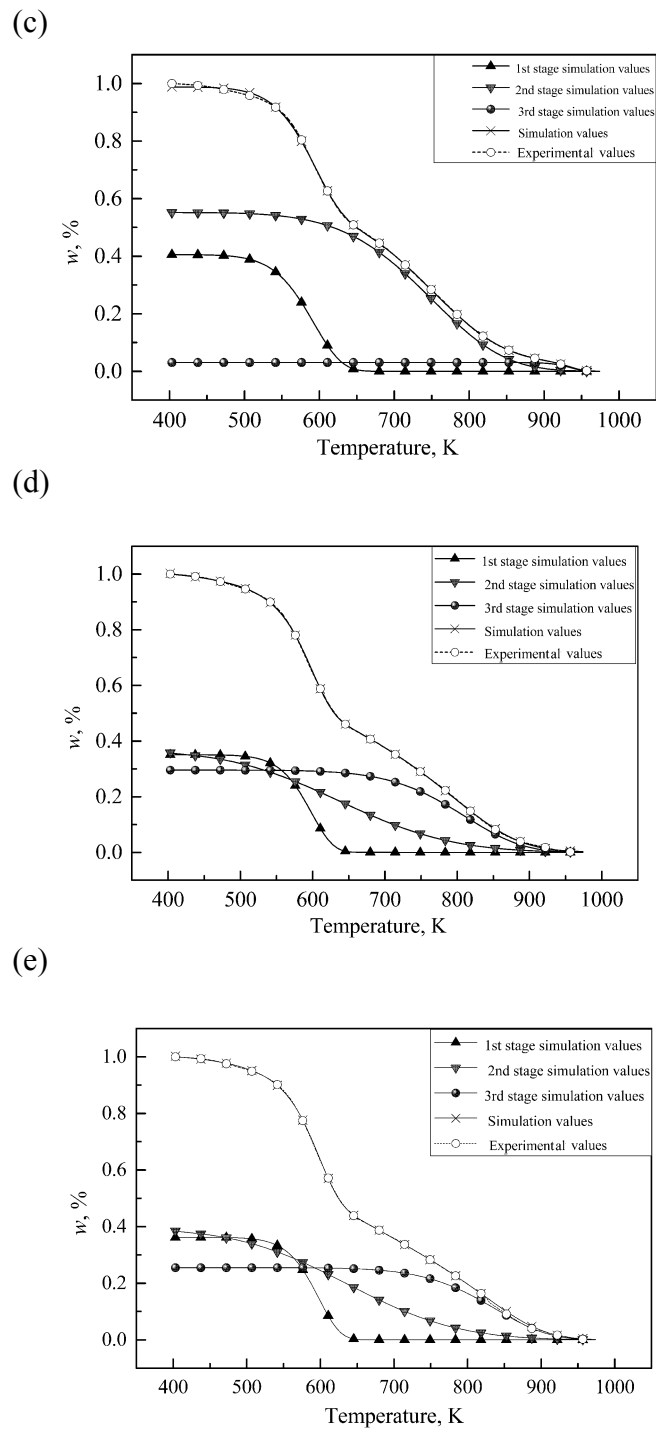
(a)

(b)

(c)

(d)

(e)
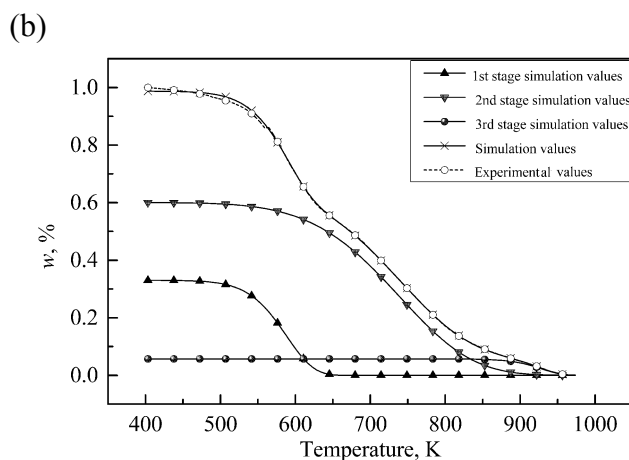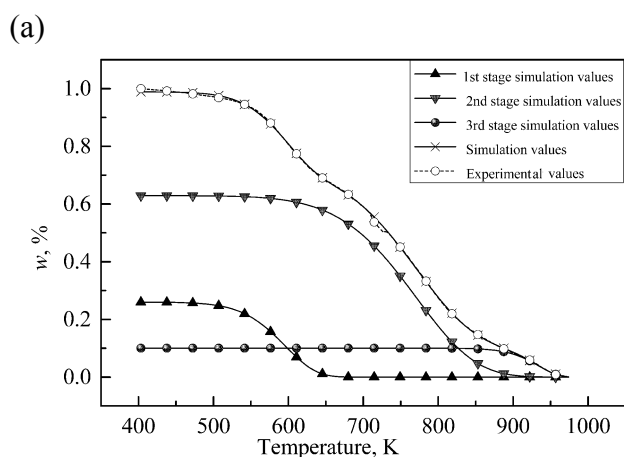
Fig. 3. TG curves simulation for blending samples: (a) M_2; (b) M_3; (c) M_4; (d) M_5; (e) M_6.

Table 3. TG curves simulation parameters for blending samples M_2–M_6

Sample	$(\Delta G_{\neq}^{\Theta})_1/$ (kJ/mol)	n_1	$(\Delta G_{\neq}^{\Theta})_2/$ (kJ/mol)	n_2	$(\Delta G_{\neq}^{\Theta})_3/$ (kJ/mol)	n_3	Correlation index r
M_2	193.82	0.38	258.95	0.27	313.09	0.87	0.999917
M_3	190.92	0.43	249.82	0.22	311.39	0.87	0.999907
M_4	192.50	0.42	253.65	0.22	313.83	1.35	0.999939
M_5	194.09	0.51	222.49	0.12	273.23	0.28	0.999984
M_6	193.89	0.53	221.59	0.14	281.92	0.32	0.999966

carbon of CS moving to a high temperature area. Moreover, from Table 3 it is clear that the free energy of activation in the first and second stages of combustion is lower than that in the third stage. The free energy of activation either favours the combustion of sample components, or decelerates it. In the first two stages of combustion the components were more apt to react than in its third stage, which accords with the simulation results shown in Figure 3.

5. Analysis of energy of activated molecules in the combustion reactions of SC/CS

The effective collision of activated molecules is an essential condition for the combustion reaction of solid particles, the energy generated from the collision of such molecules accelerates the process. Hence, it is important to investigate this energy to understand the mechanism of the whole combustion reaction. The energy of activated molecules is a kind of triplet consisting mostly of three components: activation enthalpy, activation entropy and free energy of activation [8, 22].

This research mainly employed the KAS kinetics model to calculate the energy triplet of the activated molecules of a sample. Due to the complex composition and different structure of SC and CS, their co-combustion process includes numerous continuous and parallel chemical reactions [23]. The KAS kinetics model enables one to calculate the energy change in the reactions of activated molecules and describe the mechanisms of combustion reactions of blending samples.

Applying Equation (3) [8, 23], the combustion reactions of solid particles can be described as follows:

$$\frac{d\alpha}{(1-\alpha)} = \frac{1}{\beta}\frac{RT}{N_A h} \times \exp\left(\frac{\Delta S_{\neq}^{\Theta}}{R}\right) \times \exp\left(-\frac{\Delta H_{\neq}^{\Theta}}{R}\right) dT, \qquad (7)$$

where

$$G(\alpha) = \int_0^\alpha \frac{d\alpha}{1-\alpha}. \qquad (8)$$

Integrating both sides of Equation (7) gives:

$$G(\alpha) = \frac{1}{\beta} \frac{RT}{N_A h} \times \exp\left(\frac{\Delta S_{\neq}^{\Theta}}{R}\right) \times \int_{T_0}^{T} \exp\left(-\frac{\Delta H_{\neq}^{\Theta}}{R}\right) dT, \tag{9}$$

where

$$u = \Delta H_{\neq}^{\Theta} / RT. \tag{10}$$

From Equation (10) we can get:

$$T = \Delta H_{\neq}^{\Theta} / Ru. \tag{11}$$

Differentiating Equation (11) yields:

$$dT = -(\Delta H_{\neq}^{\Theta} / Ru^2) du. \tag{12}$$

Now, substituting Equation (12) in Equation (9) gives:

$$G(\alpha) = \frac{1}{\beta} \frac{R^2 T}{\Delta H_{\neq}^{\Theta} N_A h} \times \exp\left(\frac{\Delta S_{\neq}^{\Theta}}{R}\right) \times \int_{\infty}^{u} -\frac{e^{-u}}{u^2} du. \tag{13}$$

Integrating by parts of $\int_{\infty}^{u} (-e^{-u}/u^2) du$ and approximating the result gives:

$$\int_{\infty}^{u} (-e^{-u} / u^2) du = -e^{-u} / u^2. \tag{14}$$

Substituting Equation (14) in Equations (3)–(12), the logarithm of both sides of the substituted results yields:

$$\ln \frac{\beta}{T^2} = -\frac{\Delta H_{\neq}^{\Theta}}{RT} + \ln\left(\frac{R^2 T}{\Delta H_{\neq}^{\Theta} N_A h} \exp\left(\frac{\Delta S_{\neq}^{\Theta}}{R}\right)\right) \frac{1}{G(\alpha)}. \tag{15}$$

Figure 4 shows the energy triplet curves of the activated molecules of samples M_1, M_3, M_4, M_5, M_7. As seen in Figures 4a and 4b, the curves undergo three major changes. At a conversion rate α less than 0.16, the activation enthalpy and entropy curves exhibit a sharp rise after a decline. At a conversion rate α between 0.16 and 0.6, the curves show slightly changing "platforms", and with increasing CS in the blend, the "platforms" are elevated and widened. At a conversion rate α higher than 0.6, the curves experience a sharp decline. As shown in Figure 4c, in the whole co-combustion process of the samples, the free activation energy curves show a declining trend with increasing CS in the blend. The curves depicted in Figure 4 demonstrate once again that the co-combustion of Huadian oil shale retorting residue and cornstalks is a multistage process, involving three major phases. These include the release and combustion of volatile
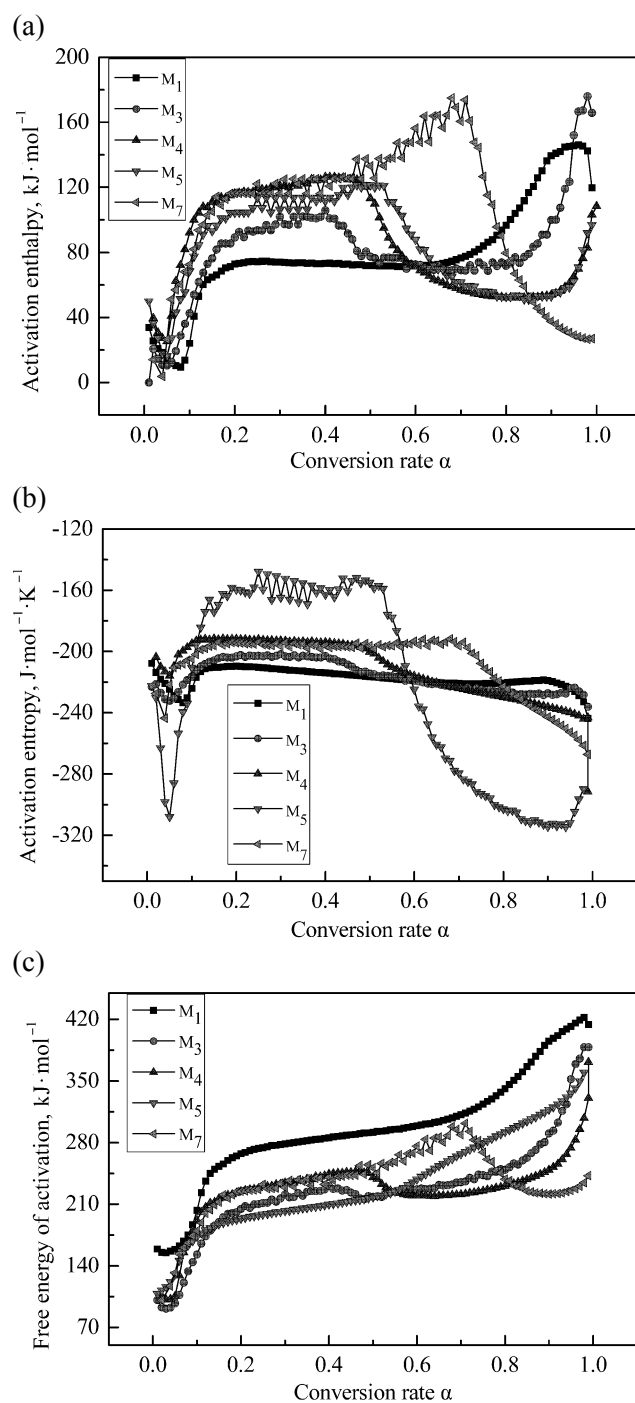
(a)

(b)

(c)

Fig. 4. Energy triplet variation curves of activated molecules of different blending samples: (a) activation enthalpy; (b) activation entropy; (c) free energy of activation.

substances of CS occurring at α = 0–0.16, the co-combustion of fixed carbon of CS and volatile of SC taking place at α = 0.16–0.6, and the combustion of fixed carbon of SC happening at α = 0.6–1.0 [24–26].

The activation entropy is or is not an intuitive response of order to the activated molecules of the activated complex, the smaller its value is, the more improved the order of the structure of activated molecules is. The activation enthalpy reflects the heat possessed by the activated molecules of the activated complex. The free energy of activation means the energy required by a thermodynamic process to take place [22]. As seen in Figures 4a–c, the activation enthalpy, activation entropy and free energy of activated molecules in different stages of co-combustion change. So, with increasing blending ratio of CS, the activation enthalpy increased, while the activation entropy and free energy of activation decreased. This trend is particularly apparent in the second stage of co-combustion (α = 0.16–0.6). In this stage, the activation entropy changed from –210 J/(mol·K) to –194 J/(mol·K), the free energy of activation decreased from 290 kJ/mol to 207 kJ/mol, and the activation enthalpy increased from 73 kJ/mol to 126 kJ/mol. The decrease of the activation entropy indicates that with increasing CS in the blend, the order of the structure of activated molecules in the co-combustion processes improves, which leads to the more orderly reactions of co-combustion. The decrease of the free energy of activation and the increase of the activation enthalpy indicate that with increasing CS in the blend, the number and collision strength of activated molecules in the co-combustion processes, as well as the energy released increase, which accelerates the whole co-combustion process. Comparison shows these results to be very similar with those obtained for the TG simulation of the above samples, which confirms the accuracy of calculations.

6. Conclusions

(1) In this research, projects of the co-combustion of SC and CS are presented. A thermogravimetric analyzer (TGA) was used to investigate the process in more detail. It was found that with increasing blending ratio of CS, the curves of co-combustion moved to low temperature areas, while the burnout temperature as well as burnout time of samples decreased, and the combustion performance of SC improved.

(2) Based on the curvature changes of TG curves and the multi-peaks and -shoulders of DTG curves, it can be concluded that the combustion of the blending samples of complex composition represented a multi-stage process of burning. The change of the free energy of activation in the components combustion was calculated on the basis of the Avrami conversion theory. The results showed that with increasing blending ratio of CS, the interaction effects of components in stages 1 and 2 of the process

were more pronounced, and the free energy of activation was evidently lower than that in stage 3.

(3) Combining thermal analysis kinetics with the classical theory of thermo-dynamics and employing the KAS equation, the change of the energy triplet of activated molecules in the co-combustion of SC and CS was investigated in more detail. Results showed that with increasing blending ratio of CS, the order of the structure of activated molecules improved, their strength of collision increased and the activation entropy decreased, but nevertheless, the burning was vigorous. The free energy of activation expresses the ease or complexity of a reaction. In this work, its values in stages 1 and 2 of combustion were lower than that in stage 3. This is in agreement with the numeric change rule presented in conclusion (2) above and reflects the accuracy of calculations.

Acknowledgements

REFERENCES

1. Giereo, R., Stille, P. *Energy, Waste and the Environment: A Geochemical Perspective.* The Geological Society Publishing House, London, 2004, 263–284.
2. Trikkel, A., Kuusik, R., Martins, A., Pihu, T., Stencel, J. M. Utilization of Estonian oil shale semicoke. *Fuel Process. Technol.,* 2008, **89**(8), 756–763.
3. Brendow, K. Global oil shale issues and perspectives. *Oil Shale,* 2003, **20**(1), 81–92.
4. Kuusik, R., Martins, A., Pihu, T., Pesur, A., Kaljuvee, T., Prikk, A., Trikkel, A., Arro, H. Fluidized-bed combustion of oil shale retorting solid waste. *Oil Shale*, 2004, **21**(3), 237–248.
5. Gil, M. V., Casal, D., Pevida, C., Pis, J. J., Rubiera, F. Thermal behaviour and kinetics of coal/biomass blends during co-combustion. *Bioresource Technol.,* 2010, **101**(14), 5601–5608.
6. Zanoni, M. A. B., Massard, H., Martins, M. F. Formulating and optimizing combustion pathways for oil shale and its semi-coke. *Combust. Flame,* 2012, **159**, 3224–3234.
7. Wang, Q., Wang, H. G., Sun, B. Z., Bai, J. R., Guan, X. H. Interactions between oil shale and its semi-coke during co-combustion. *Fuel,* 2009, **88**(8), 1520–1529.
8. Wang, Q., Zhao, W. Z., Liu, H. P., Jia, C. X., Li, S. H. Interactions and kinetic analysis of oil shale semi-coke with cornstalk during co-combustion. *Appl. Energ.,* 2011, **88**, 2080–2087.

9. Sun, B.-Z., Wang, Q., Shen, P.-Y., Qin, H., Li, S.-H. Kinetic analysis of co-combustion of oil shale semi-coke with bituminous coal. *Oil Shale,* 2012, **29**(1), 63–75.

10. Chen, L. H., Li, X. B., Wen, W. Y., Jia, J. D., Li, G. Q., Deng, F. The status, predicament and countermeasures of biomass secondary energy production in China. *Renewable and Sustainable Energy Reviews,* 2012, **16**, 6212–6219.

11. Wang, C. P., Wang, F. Y., Yang, Q. R., Liang, R. G. Thermogravimetric studies of the behavior of wheat straw with added coal during combustion. *Biomass Bioenerg.,* 2009, **33**(1), 50–56.

12. Sultana, A., Kumar, A. Ranking of biomass pellets by integration of economic, environmental and technical factors. *Biomass Bioenerg.,* 2012, **39**, 344–355.

13. Nimmo, W., Daood, S. S., Gibbs, B. M. The effect of O_2 enrichment on NO_x formation in biomass co-fired pulverized coal combustion. *Fuel*, 2010, **89**(10), 2945–2952.

14. Syed, S., Qudaih, R., Talab, I., Janajreh, I. Kinetics of pyrolysis and combustion of oil shale sample from thermogravimetric data. *Fuel,* 2011, **90(4)**, 1631–1637.

15. Garcia, A. N., Font, R. Thermogravimetric kinetic model of pyrolysis and combustion of an ethylene-vinyl acetate copolymer refuse. *Fuel,* 2004, **83**(9), 1165–73.

16. Várhegyi, G., Szabó, P., Jakab, E., Till, F., Richard, J.-R. Mathematical modeling of char reactivity in Ar-O_2 and CO_2-O_2 mixtures. *Energ. Fuel.,* 1996, **10**(6), 1208–1214.

17. Yinnon, H., Uhlmann, D. R. Applications of thermoanalytical techniques to the study of crystallization kinetics in glass-forming liquids, part I: Theory. *J. Non-cryst. Solids,* 1983, **54**(3), 253–275.

18. Afify, N. Calorimetric study on the crystallization of a $Se_{0.8}Te_{0.2}$ chalcogenide glass. *J. Non-cryst. Solids,* 1992, **142**, 247–259.

19. Finney, E. E., Finke, R. G. Is there a minimal chemical mechanism underlying classical Avrami-Erofe'ev treatments of phase-transformation kinetic data? *Chem. Mater.,* 2009, **21**(19), 4692–4705.

20. Kreevoy, M. M., Truhlar, D. G. *Transition State Theory in Investigation of Rates and Mechanisms of Reactions.* John Wiley & Sons, New York, 1986.

21. Spencer, J. N., Bodner, G. M., Rickard, L. H. *Chemistry – Structure & Dynamics.* John Wiley & Sons, New York, 2010.

22. Atkins, P. W. *Physical Chemistry.* Oxford University Press, Oxford, 1998.

23. Starink, M. J. The determination of activation energy from linear heating rate experiments: a comparison of the accuracy of isoconversion methods. *Thermochim. Acta*, 2003, **404**(2), 163–176.

24. Yao, F., Wu, Q. L., Lei, Y., Guo, W. H., Xu, Y. J. Thermal decomposition kinetics of natural fibers: Activation energy with dynamic thermogravimetric analysis. *Polym. Degrad. Stabil.,* 2008, **93**(1), 90–98.

25. Ozawa, T. A new method of analyzing thermogravimetric data. *Bull. Chem. Soc. Jpn.*, 1965, **38**(11), 1881–1886.

26. Oza, S., Ning, H., Ferguson, I., Lu, N. Effect of surface treatment on thermal stability of the hemp-PLA composites: Correlation of activation energy with thermal degradation. *Compos. Part B-Eng.,* 2014, **67**, 227–232.